Insights on the C2 and C3 electroconversion in alkaline medium on Rh/C catalyst: in situ FTIR spectroscopic and chromatographic studies

Thamyres Fernandes Messa Moreira, Kouakou Boniface Kokoh, T. W. Napporn, Paulo Olivi, Cláudia Morais

Insights on the C2 and C3 Electroconversion in Alkaline Medium on Rh/C catalyst: *in situ* FTIR Spectroscopic and Chromatographic Studies

Thamyres Fernandes Messa Moreira [1,2], Kouakou Boniface Kokoh[2], Teko Wilhelmin Napporn[2], Paulo Olivi[1], Cláudia Morais[2]*

[1]*Laboratório de Eletroquímica e Eletrocatálise Ambiental, Departamento de Química da Faculdade de Filosofia Ciências e Letras de Ribeirão Preto, Universidade de São Paulo, Av. Bandeirantes, 3900, 14040-901 Ribeirão Preto, SP, Brazil,*

[2] *Université de Poitiers, IC2MP UMR 7285 CNRS, 4 rue Michel Brunet, B27, TSA 51106, 86073 Poitiers Cedex 09, France*

*Corresponding author: claudia.gomes.de.morais@univ-poitiers.fr;

HIGHLIGHTS:

- Carbon-supported Rhodium catalyst synthesis by Bromide Anion Exchange (BAE) method;
- CO oxidation on Rh/C starts with linearly adsorbed (CO_L) oxidation at 0.35 V *vs.* RHE;
- Ethanol Oxidation Reaction (EOR) on Rh/C facilitates the C_1 products selectivity;
- Glycerol Oxidation Reaction (GOR) with preferential glycerate ion formation;

Graphical Abstract:

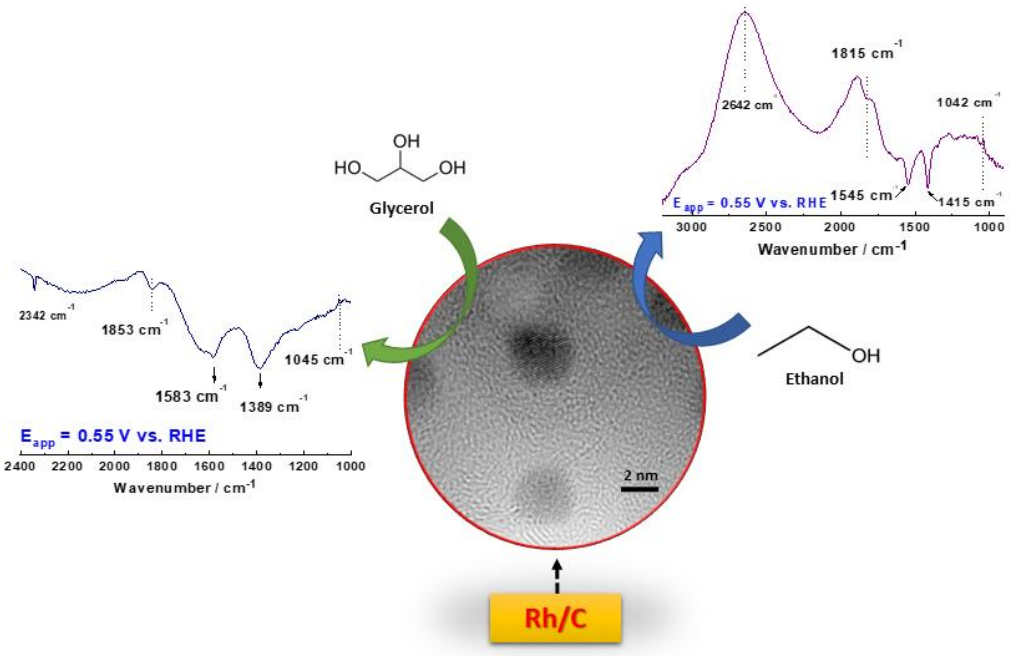

ABSTRACT

The present work evaluates ethanol and glycerol electro-oxidation on Rh/C catalysts prepared using the Bromide Anion Exchange (BAE) method. Physicochemical characterizations were performed using Thermogravimetric Analysis (TGA), X-ray diffraction (XRD), and X-ray photoelectron spectroscopy (XPS). The SPAIRS investigations revealed that the CO adsorption modes on Rh sites occur on the linearly adsorbed CO (CO_L) and bridged bonded (CO_B) modes. In ethanol oxidation reaction (EOR), the Rh effect was evaluated by analyzing the products generated after bulk electrolysis using High-Performance Liquid Chromatography (HPLC) and in situ FTIR spectroscopy. The results confirmed the C-C cleavage Rh ability at low potentials and revealed that EOR follows both reaction pathways on Rh/C. While in glycerol oxidation reaction (GOR), Rh addition increases high added-value products formation such as glycerate ion. The GOR main route follows the glyceraldehyde pathway. The results highlighted that Rh is a good candidate for ethanol and glycerol electrochemical conversion at low potentials.

Keywords: Ethanol, Glycerol, Rhodium, FTIR spectroelectrochemistry, Chromatographic analysis, Alkaline medium

1. Introduction

Direct Alcohol Fuel cells (DAFCs) are well known devices for the chemical energy conversion stored in fuels into electricity [1, 2]. Due to increasing energy demand and environmental concerns there is a growing interest in such devices based on renewable energy resources [3]. A significant challenge in making DAFCs attractive is the production of anodes that allow complete alcohol oxidation to CO_2 with high efficiency [1]. Therefore, the catalyst's role in the kinetic process is crucial to improve DAFCs anode performance, and thus the metal composition is an important parameter to develop anode catalysts [2, 4-6].

Platinum (Pt) is widely reported as a highly active catalyst for alcohol oxidation reactions [7-11]. Nevertheless, the Pt surface is easily poisoned by intermediate species such as adsorbed CO and CH_x which considerably decrease the reaction rate process [12]. To overcome this issue, several studies focus on using bimetallic platinum-based catalysts. Therefore, metals such as Cobalt (Co) [13, 14], Ruthenium (Ru) [15-17], Copper (Cu) [18-21], Tin (Sn)[22, 23], Nickel (Ni) [24-29], Niobium (Nb)[30], Molybdenum (Mo)[31], Rhodium (Rh) [32-37], and others [38-40], are reported as co-catalysts on alcohol oxidation reaction. These metals are suitable to promote a bifunctional mechanism through hydroxyl ions formation at a low potential, improving the oxidative alcohol conversion [22].

Rh was previously described as an active co-catalyst for Ethanol Oxidation Reaction (EOR) and Glycerol Oxidation Reaction (GOR) [35, 41-46]. For example, Juan Bai *et al*. [42] studied the PtRh/C catalyst for EOR and concluded that the bimetallic catalyst displayed high activity and durability, particularly in alkaline medium, which was attributed to composition and morphological effects. Concerning the GOR studies, Long Huang *et al.* [47] tested PtRh/C catalysts using in situ FTIR and ^{13}C NMR spectroscopies to investigate the reaction mechanism.

The authors concluded that compared to Pt/C, the PtRh bimetallic composition shows higher activity and favors the tartronic acid formation at high potentials.

Although the bimetallic catalysts have shown important benefits improving the catalytic activity, the study of Rh role as monocatalyst still requires more highlights. Some authors reported that Rh as a monometal composition has a low electrochemical activity for EOR in an acidic solution [34, 42]. Nevertheless, in alkaline medium, Fangfang Zhang *et al.* [48] demonstrated that Rh is active for EOR. Furthermore, the results indicated that Rh/C negatively shifts the EOR onset potential, presenting more selectivity for CO_2 formation than the Palladium catalyst (Pd/C). Yange Suo and I-Ming Hsing [49] reported the Rh/C behavior for EOR in alkaline medium with impedance spectroscopy measurements. The results suggested that Rh/C exhibits a higher activity for ethanol oxidation at low potentials, and the reaction pathway differs to that on the Pd/C catalyst. However, for both studies, the reaction mechanism was not probed.

The main Rh effect on GOR is still not completely elucidated. Rodrigues *et al.* [50] prepared Rh/C catalyst for GOR concluding that Rh is active for this reaction, and in the presence of more oxygenated species increases the Glyceric acid selectivity at high pressure conditions. Meantime, more analyses are required to describe the reaction mechanism. Thus, it is essential to improve the understanding of the reaction mechanism of the small organic molecules on the Rh catalyst. Furthermore, several characterizations studies dealt with ethanol or glycerol electrooxidation on single crystal or polycrystalline electrodes. The characterization of supported catalysts or fuel cell membrane electrode assemblies (MEAs) is thus essential to further investigate this topic.

Electrochemical methods coupled with analytical and spectroscopic methods such as High-Performance Liquid Chromatography (HPLC), Differential Electrochemical Mass Spectrometry (DEMS), Electrochemical Thermal Desorption Mass Spectroscopy (ECTDMS),

and *in situ* Fourier Transform Infrared Spectroscopy (FTIRS) were shown to be extremely helpful to identify the adsorbed intermediates on the catalyst surface [31, 47, 51-53]. These combinations enable to better understand the selectivity of the reaction process, consequently, improving the anode catalyst's development. Despite this, the literature using *in-situ* FTIR to elucidate the alcohol oxidation mechanism reaction with Rh/C catalysts in alkaline medium is sparse. The main reports are related to Pd and Pt-based catalysts [43, 52, 54-57]. The main aim of the present study is therefore to explore the role of Rh supported catalyst on ethanol and glycerol oxidation reactions by coupling electrochemical measurements to HPLC analyses and *in situ* FTIR spectroscopy for a straightforward identification of products and intermediates generated during the reactions.

2. Experimental

2.1 Chemicals

Rhodium (III) chloride hydrate ($RhCl_3.xH_2O$, Rh basis $\geq$ 38%), sodium borohydride ($NaBH_4$, 99%), and potassium bromide (KBr, 99%) were purchased from Sigma-Aldrich and used as received. For electrochemical characterizations, Ethanol (C_2H_6O, 99%) was obtained from Merck, and Sodium hydroxide (NaOH, 98%), and glycerol (ReagentPlus > 99%,) were purchased from Sigma-Aldrich. Acetic acid, tartronic acid, glyceric acid, glycolic acid, glyoxylic acid, oxalic acid, formic acid, and sodium carbonate used was purchased from Sigma-Aldrich, and utilized without further purification. Vulcan XC 72R Carbon used as supporter was purchased from Cabot, and pre-treated in a tubular oven at 900 ºC for 5 hours in argon flow [34]. Millipore Milli-Q1 water (18.2 MΩ cm at 20 ºC) was used in all prepared solutions.

2.2 Catalysts synthesis

The Rh/C catalyst was prepared following the BAE synthesis method protocol [25, 58]. This synthesis route promotes the reduction of a precursor metal ion (in the complex state) in aqueous solution using bromide ion as capping agent. The Bromide anion exchange promotes through its size a great steric effect stabilizing the particle during the reduction process with sodium borohydride. Thereby, to develop the electrocatalysts this method is considered a cleaner, simple, relatively low-cost synthesis method.

Parameters such as the metal salt concentration, the volume of reaction, the amount of reducing agent and the temperature were set as reported in the state-of-the-art BAE protocol[59]. The ratio ϕ = n(KBr)/n(metal (s)), amount of reducing agent, and the temperature are fixed in 1.0 mmol L^{-1}, 100.0 mL, 1.5, 15-fold excess and 40.0 ºC, respectively, and respecting a metal loading of 20 wt. % [58]. Thus, an appropriate amount of rhodium chloride salt was dissolved in 100.0 mL water followed by the potassium bromide addition under vigorous stirring for 1 h. Then, carbon Vulcan was added and the resulting solution was homogenized in ultrasound bath for 45 min. A fifteen-fold excess of sodium borohydride ($NaBH_4$) was dissolved in cold water and then, dropwise added into the mixture and stirred for 2 h at 40 °C. Finally, the resulting product was filtered and exhaustively washed with ultrapure water. The catalyst powder was dried at 40 ºC for 12 h. The Rh/C catalyst was physicochemical characterized by X-ray diffraction, thermogravimetric analysis (TGA), and X-ray photoelectron spectroscopy.

2.3 Physicochemical characterization

The Rh/C metal-loading was confirmed by thermogravimetric analysis (TGA) on a Q600 TA Instruments SDT2960 under synthetic air using a 10 °C min^{-1} heating rate from 20 to 900 °C. X-ray diffraction pattern was obtained with an X-ray diffractometer (Bruker - D2 Phaser) operating with Cu Kα radiation (λ = 0.15406 nm) generated at 30 kV and 10 mA. The parameters were kept constant during the analysis: 2θ range = 20 - 90º, and step = 0.025º s^{-1}. Debye-Scherrer equation was used to estimate the crystallite size, and the unit cell parameters were determined using the least-squares method of the UFit.exe v1.3-1992 software. High-Resolution Transmission Electron Microscopy (HRTEM) was used to investigate the surface morphology with a TECNAI G2F20 electron microscope in bright and dark field modes. The nanoparticles size distribution was set by examining more than 300 free particles. X-ray photoelectron spectroscopy (XPS) was used to probe and characterize the surface and Rhodium oxidation states. Analyses were performed on a Kratos Axis Ultra DLD spectrometer equipped with a monochromatic Al Kα X-ray source (1486.6 eV) operating at 15 kV and 10 mA (150 W). The analysis spot size is approximatively 300 µm x 700 µm and the pass energy is 20 eV for recording high resolution spectra. The XPS data were calibrated by using the C1s (C-C) peak binding energy (B.E.) at 284.6 eV, and the spectra were fitted with CasaXPS software (version 2.3.17). Shirley background has been chosen and asymmetric Gaussian-Lorentzian profile functions were used to fit the spectra. The base pressure of the instrument was 9 x 10^{-8} Pa and the sample powder was pressed in a copper holder of 3 mm diameter and introduced into the preparation chamber after being outgassed overnight.

2.4 Electrochemical characterization

For the electrochemical experiments, a glassy carbon (GC) disk (3 mm diameter) electrode coated with 3 µL of the catalytic ink was used as the working electrode. This ink was prepared dispersing 2.0 mg of the catalyst powder in a solution composed of water (100 µL), isopropanol (95 µL) and a Nafion® suspension (5 µL) (5 wt.% in aliphatic alcohols, Aldrich). Sequentially, this ink was homogenized in an ultrasound bath for 30 min.

The measurements were performed at room temperature (T = 25 °C) using an Autolab PGSTAT 302 N potentiostat. $Hg/HgO/OH^-$ (0.1 mol L^{-1} NaOH) and a glassy carbon slab were used as the reference and counter electrodes, respectively. In this study all potentials are referred to the reversible hydrogen electrode (RHE). Cyclic voltammetry (CV) and chronoamperometry (CA) were performed in a conventional three-electrode cell. The supporting electrolyte is a 0.10 mol L^{-1} NaOH solution and the CVs were recorded by potential cycling from 0.12 to 1.15 V *vs.* RHE. The CO stripping voltammetry was performed by purging carbon monoxide (CO) gas for 5 min while holding the electrode potential at 0.1 V to saturate the electrode surface with a CO_{ads} layer and then removing free CO in the cell by purging N_2. The electrocatalytic performance was evaluated using CV at a 10 mV s^{-1} scan rate and CA in solution containing 0.20 mol L^{-1} ethanol or glycerol. The chronoamperometry tests were conducted for 30 min at 0.55 V *vs.* RHE and 0.55/0.70 V vs. RHE for ethanol and glycerol, respectively. In all the tests the solutions were deoxygenated with N_2 gas for nearly 15 min before starting the electrochemical measurements.

2.6 Reaction products analysis by HPLC

Long-term electrolysis was carried out to determine the fuel (ethanol or glycerol) products in the bulk electrolytic solution by HPLC. Potentiostatic experiments were performed with potential fixed in 0.55/0.85 V *vs*. RHE and 0.55 V vs. RHE for ethanol and glycerol respectively, for 4 hours. For each electrolysis cycle, the first potential was applied following the plateau to E_{app} 0.55/0.85 V *vs*. RHE for 60 s, corresponding to the organic molecules' electrooxidation, and sequentially applying E_{reg} =1.4 V vs RHE for 2 s, promoting the electrode surface regeneration. The potential electrode variation during the electrolysis time is reported in **Figure 1S**. Thus, every 60 min an aliquot was collected and injected. The chromatograph system (Shimadzu, model LC-10AT) was coupled to a double on-line detection system with refractive index RID-10A and UV ($\lambda = 210$ nm) detectors. The analysis was performed using an automatic injector (injection volume of 20 μL) with an Aminex HPX-87H (Bio-Rad) column operating in the isocratic mode. The mobile phase was sulfuric acid (3.33 mmol L^{-1}) with a 0.6 mL min^{-1} flow rate ant the analysis was performed at 45 °C. Finally, reaction products quantitative determination was conducted by comparing retention times with pure commercial standards injected under the same analysis conditions (external calibration).

2.7 Spectroscopic determination of the intermediate species

In order to monitor the presence of intermediates and the *in situ* formation of reaction products, the SPAIRS (Single Potential Alteration Infrared Reflectance Spectroscopy) technique was used. The wavenumber range acquired was 1000–4000 cm^{-1} with a spectral resolution of 8 cm^{-1}. The experiments were carried out under external reflection conditions in a Bruker IFS66v spectrometer modified for a beam reflectance at 65° incident angle and equipped with a liquid

N_2-cooled HgCdTe detector under vacuum conditions. The cell used was especially fitted with a CaF_2 flat window tailored for in situ IR experiments. The electrochemical measurements performed were CO stripping, cyclic voltammetry and chronoamperometry, both in the presence of 0.20 mol L^{-1} ethanol or glycerol. For CO stripping and cyclic voltammetry measurements, spectra were acquired every 50 mV within potential values ranging between 0.10 and 1.2 V vs. RHE at a scan rate of 1 mV s^{-1}, while for chronoamperometry measurements spectra were acquired every 3 minutes for 30 minutes. Two different working electrodes were used in this study: a vitreous carbon substrate (8 mm diameter) for GOR and a gold substrate (disk with 7 mm diameter) for EOR and CO stripping measures. The precursor solution was deposited onto the following substrate: 5 µL of the catalytic ink, prepared in isopropanol (375 µL), water (125 µL), and (30 µL) Nafion® suspension (5 wt.% in aliphatic alcohols, Aldrich). CO adsorption was conducted by bubbling CO into 0.10 mol L^{-1} NaOH during 5 min at 0.10 V vs. RHE potential control. Sequentially, free remaining CO in solution was removed with nitrogen purge for 25 minutes. Finally, the CV was recorded to perform the oxidative behavior of the adsorbed CO monolayer between 0.10 and 1.2 V vs. RHE at 1 mV s^{-1} scan rate. The results are presented as a function of $\Delta R/R_0$ vs. wavenumber (cm). The reflectance ratio $\Delta R/R_0$ was calculated, where R and R_0 are the reflectance measured at the sample and reference potentials, respectively. These data manipulation results in spectra in which peaks pointing up arise from species consumption and peaks pointing down indicate species formation.

3. Results and discussion

3.1 Physicochemical characterization of Rh/C

The metal loading was confirmed using TG analysis. **Figure 1a** shows a typical Rh/C thermogravimetric profile [60]. Firstly, the water adsorbed on the surface was removed and

detected up to 302 ºC. The carbon support combustion starts at 302 ºC and the intended metal weight was reached after 600 ºC.

The Rh crystal phase is identified by XRD and **Figure 1b** depicts the Rh XRD pattern. Peaks at 39.7°, 46.3° and 67.4°, respectively, correspond to (111), (220), and (311) Rh face-centered cubic (*fcc*) reflection planes. The diffraction peak at around 25° corresponds to the carbon Vulcan XC-72 (002) plane. As described previously, the mean crystallite size was estimated using the Rh (111) peak according to the Debye Scherrer's equation [17]. The obtained mean size for Rh was 2.9 nm. Compared to the literature, the proposed synthetic method displays a good crystallite size correlation. For example, Ehab Sawy and Peter Pickup [61] prepared Rh/C catalyst by polyol method and the Rh average crystals were about 4.5 nm size. Additionally, Rh lattice parameter was calculated from the (111) diffraction peak positions in the XRD patterns. The Rh/C catalyst experimental lattice parameter of Rh/C is 0.3790 nm, which is very close to the theoretical value (0.3831 nm) [62].

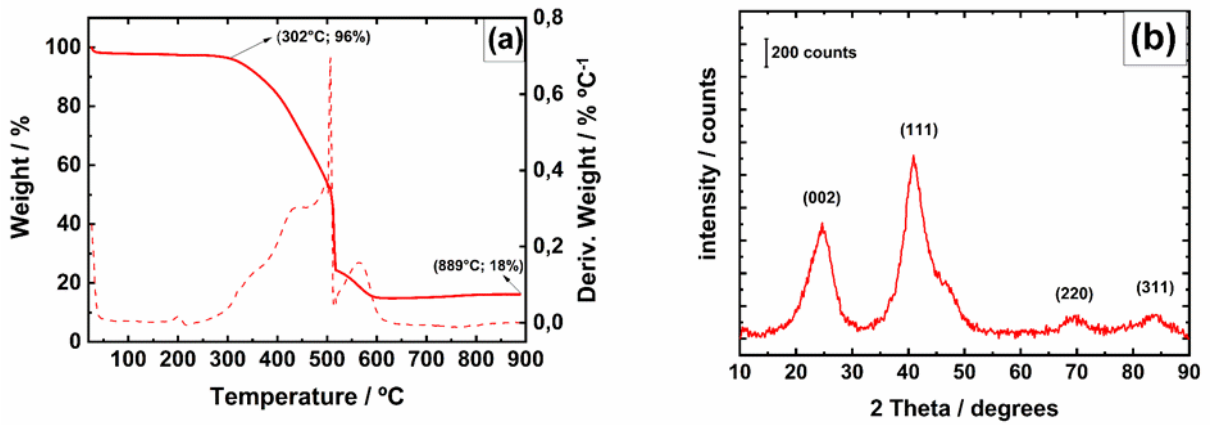

Figure 1 - (a) TGA curve for Rh/C catalyst recorded in air atmosphere, at 10 ºC min^{-1} linear temperature variation from 25 to 900 ºC; (b) XRD patterns of the carbon supported Rh/C material prepared from BAE method;

3.2 Electrochemical characterization

In order to evaluate the Rh/C electrochemical behavior, cyclic voltammetry (CV) was carried out. **Figure 2** depicts the typical CV curve in 0.10 mol L^{-1} NaOH at 10 mV s^{-1}. The CV profile shows three distinct potential regions; *i*) 0.05 – 0.35 V (vs. RHE) hydrogen desorption; *ii*) after 0.35 V (vs. RHE) the surface oxidation starts immediately evidencing the double layer charging region absence. RhO and Rh(OH) formation followed by $Rh(OH)_3$ are reported in the initial oxidation stages [63, 64]; *iii*) the peak at 0.40 V (*vs*. RHE) in the cathodic scan corresponds to the oxide reduction process. Additionally, after this peak it is clearly observed that the process is superimposed with the hydrogen adsorption region.

The CO is broadly studied as a probing molecule in order to evaluate the material ability to catalyze the alcohol oxidation reaction. To estimate the Rh effects on CO adsorption modes, CO stripping experiments were coupled with *in situ* infrared reflectance spectroscopy by the SPAIRS method, which consists in acquiring FTIR spectra at 50 mV intervals during linear scanning at 1 mV s^{-1}. **Figure 2b** depicts the representative SPAIRS spectra recorded in the region between 2400 and 1000 cm^{-1} during the CO stripping. The CO spectra were calculated taking as reference a spectrum at 1.15 V (vs. RHE), where CO is completely oxidized, and the intensities of the negative-going bands are proportional to the CO coverage at the respective potential **(Figure 3S)**. The water O–H bending mode band appears at 1640 cm^{-1} [65]. The main bands observed at 1965 and 1856 cm^{-1} are attributed to linearly adsorbed CO (CO_L) and the bridged bonded one (CO_B) on Rh sites, respectively [66-69]. The CO_B adsorption was reported previously in the bridging carbonyls band on Rh^0 [67], while the CO_L adsorption mode is associated with the reduction process of Rh^{3+} to Rh^+, which occurs on the catalyst surface during the CO adsorption at low temperatures [67, 70]. This is in good agreement with the XPS results (**Figure 2S**) that revealed these two oxidation states for Rh (Rh^{3+} and Rh^0).

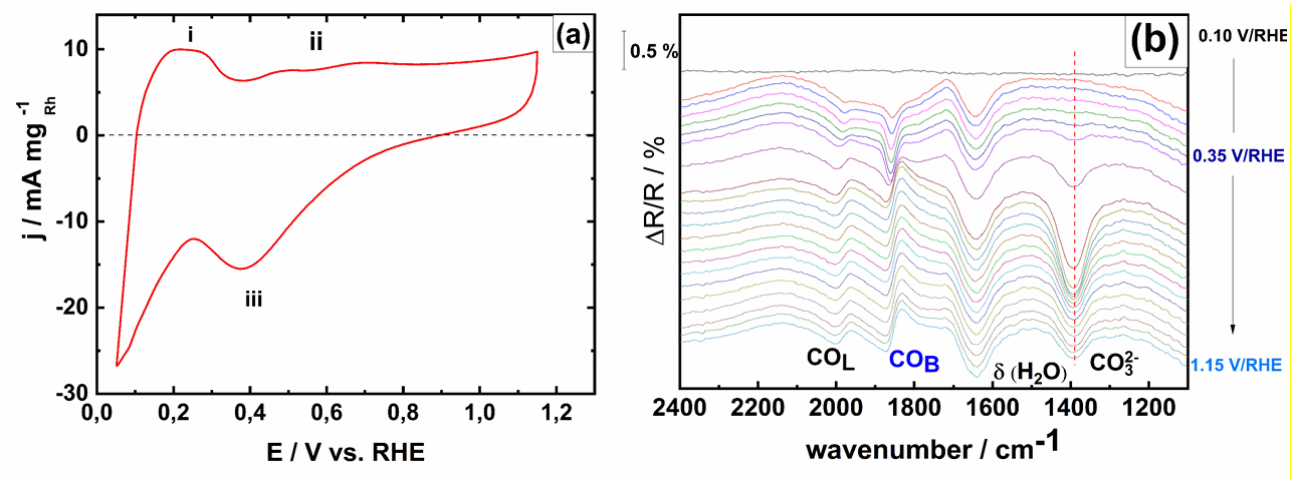

Figure 2 – (a) Typical Rh/C voltammogram (CV) recorded in 0.10 mol L^{-1} NaOH at 10 mV s^{-1}; **(b)** SPAIR spectra of the species from CO oxidation in 0.1 mol L^{-1} NaOH on Rh/C. Reference spectrum taken at 0.10 V vs. RHE;

3.3 Ethanol Oxidation Reaction (EOR)

Figure 3a shows the EOR linear polarization curve in the potential range of 0.05 – 1.2 V *vs.* RHE. Firstly, it is possible to confirm that Rh/C is active for EOR in alkaline medium, indicating the Rh ability of generating hydroxyl (HO^-) species on the surface. The EOR starts at 0.17 V, and two different peaks were observed during the forward scan at 0.60 V and 0.76 V vs. RHE in agreement with previous studies and are related to the chemisorbed species oxidation from ethanol adsorption [19, 41, 71].

The reaction pathways investigation was carried out by electrolysis coupled with HPLC and in situ FTIR analyses. The chronoamperometry tests were performed in a 0.10 mol L^{-1} NaOH N_2-deoxygenated solution containing 0.20 mol L^{-1} ethanol during 4 hours in two different potential regions: 0.55 V and 0.85 V vs. RHE. The HPLC set-up was equipped with a refractive index detector, which allowed us to use external calibration to determine the concentration of carbonate that was produced. **Table 1** shows the reaction products distribution resulting from the ethanol conversion after 4 hours of electrolysis. The ethanol consumption reaches 20 and 27% at 0.55 and 0.85 V vs. RHE, respectively. The acetate ion (CH_3COO^-) was the major

product and for both applied potential conditions, the CO_3^{2-} formation ability was confirmed. Based on previous reports, the acetaldehyde detection is difficult in alkaline medium due to the aldolization reaction [72]. Nevertheless, the mass balance on **Table 1** suggests the acetaldehyde compound presence in the electrolytic solution, even though in a low amount. The main explanation might be due to the acetaldehyde electrochemical transformation into acetate or a nucleophilic attack by HO^- leading to acetate [73]. By comparing the reaction products, it was possible to verify that at high potential values (0.85 V vs RHE) the CH_3COO^- formation increases as well as the CO_3^{2-} one.

Table 1: Reaction products distribution issued from EOR on Rh/C at different potentials after 4 hours.

E_{app} (V) (*vs.* RHE)	Ethanol conversion (%)	Reaction Products		Mass balance (%)
		Acetate ion (%)	CO_3^{2-} (%)	
0.55	20	67	6	73
0.85	27	78	8	86

In Situ Infrared Reflectance Spectroscopy Measurements

The FTIR analysis is important to provide information on the reaction mechanism process. **Figure 3b** displays the SPAIR spectra obtained during ethanol oxidation in the potential range of 0.05 – 1.20 V vs. RHE. The ethanol consumption due to the oxidation is indicated by the up-going IR band at 1049 cm^{-1} characteristic of ethanol (C–O stretch) vibration [51]. On the same time the band assigned around 2614 cm^{-1} is also associate to the ethanol oxidation due to OH^- species consumption [31].

At 0.15 V vs. RHE a down-going band at 1815 cm^{-1} is assigned to CO_B on Rh [72]. Moreover, acetate ion (CH_3COO^-) formation is confirmed by the bands at 1409, and 1553 cm^{-1} [52, 72-74], starting at 0.45 V *vs.* RHE. Nevertheless, it is easily observed that the band shape at 1553 cm^{-1} is affected by the water O–H bending mode (1645 cm^{-1}). As a consequence, **Figure 3b** is not convenient to evaluate the CO_3^{2-} formation based on relative intensities of the bands at 1409 cm^{-1} and 1553 cm^{-1}, since the water O–H bending distorts the natural shape on the acetate band at 1553 cm^{-1} [72].

Thereafter, we accomplished FTIRS measurements to obtain additional evidence of the reaction products detected by HPLC. For this purpose, we employed SPAIRS by coupling with a chronoamperometry experiment at 0.55 and 0.85 V *vs* RHE for 30 min in the presence of 0.20 mol L^{-1} ethanol in 0.10 mol L^{-1} NaOH. **Figure 3c** shows the resulting spectra obtained during 3 to 30 min of reaction at 0.55 V vs. RHE. Firstly, it is observed that a band at 1836 cm^{-1} indicates that CO_B is still adsorbed at the catalyst surface at this potential. This emphasizes the C-C bond cleavage and the dissociative ethanol adsorption on Rh/C at low potentials. Sheng *et.al* [75] demonstrated that the Rh contribution is related to the OH* formation, which increases the CO_3^{2-} surface selectivity. Furthermore, under high potentials the OH* coverage on Rh sites is more accentuated than that on Pt. Consequently, the β-dehydrogenation [75] is facilitated at low potentials increasing the electrochemical oxidation on Rh surface. At 0.55 V vs. RHE CH_3COO^- remains the main reaction product. However, it is possible to verify that the band shape at 1409 cm^{-1} is not symmetrical compared with the reference material **(Figure 4S),** and its intensity is significantly higher than the band at 1553 cm^{-1} [52], while these intensities are quite similar in the reference spectrum. This change in the band's shape and relative intensity is associated with CO_3^{2-} species formation when ethanol is oxidized [72]. Indeed, the CO_3^{2-} ion shows a band at 1390 cm^{-1} (reference spectrum **in Figure 4S)**, which is therefore hidden by acetate ions band at 1409 cm^{-1}. **Figure 3d** shows the FTIR spectra acquired during

ethanol oxidation on Rh/C at 0.85 V vs. RHE during 30 min, and the same compounds to those obtained at 0.55 V vs. RHE are detected. It is important to stress that the CO_B is still adsorbed on the Rh surface at this potential, emphasizing the catalyst C-C bond cleavage ability during all the studied potential ranges.

The ethanol oxidation mechanism is complex, involving many intermediates. However, combining the HPLC results with the FTIR in situ investigations, the two main reported EOR pathways must be considered for EOR on Rh/C [37, 49, 76-78]:

(i) The acetate pathway involving 4 electrons keeps the molecule skeleton -C-C bond [79, 80]. Herein the intermediate is acetaldehyde which could not be directly observed but its presence was suggested by mass balance of the remaining reaction products from HPLC results of **Table 1**;

(ii) The second route involves the C-C bond cleavage, herein revealed by FTIR results, the CO_B presence during the EOR evaluation was the evidence of the Rh ability to enable the C_1 products selectivity [72, 78].

Additionally, another influence in the reaction pathway is the water adsorption on the Rh site, which is stronger than that observed on Pt site. This can affect the dehydrogenation reaction decreasing the acetate pathway efficiency and favors the complete ethanol oxidation [75].

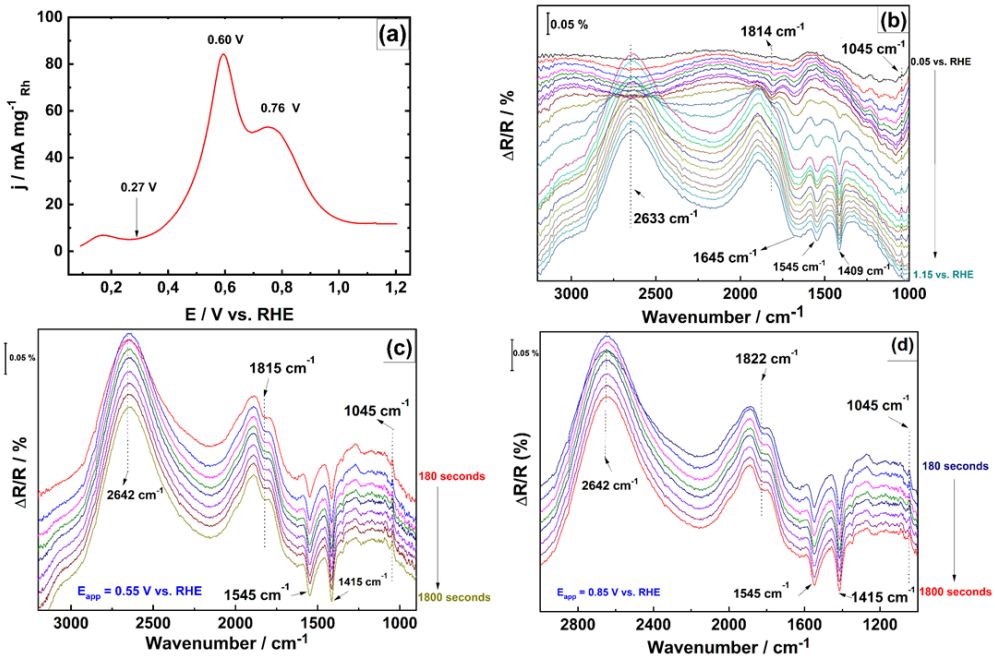

Figure 3: (a) EOR polarization curve oxidation on Rh/C catalyst at 10 mV s^{-1} in 0.1 mol L^{-1} NaOH electrolytic solution containing 0.2 mol L^{-1} Ethanol; **(b)** SPAIR spectra recorded in 0.1 mol L^{-1} NaOH electrolyte containing 0.2 mol L^{-1} of ethanol at 1 mV s^{-1} in the potential range 0.10 - 1.20 V vs RHE; **(c)** FTIR spectra recorded during chronoamperometry in 0.1 mol L^{-1} NaOH + 0.2 mol L^{-1} ethanol at 0.55 V vs. RHE; **(d)** FTIR spectra recorded during chronoamperometry in 0.1 mol L^{-1} NaOH + 0.2 mol L^{-1} ethanol at 0.85 V vs. RHE.

3.4 Glycerol oxidation Reaction (GOR)

Figure 4a depicts the polarization curve of glycerol oxidation on the Rh/C material. The GOR was investigated in 0.10 mol L^{-1} NaOH containing 0.20 mol L^{-1} glycerol between 0.05 – 1.2 V vs. RHE potential range. Firstly, it is essential to note that Rh/C was active towards glycerol oxidation at low onset potential, starting at 0.26 V vs. RHE, and the main oxidation peak is observed during the forward scan at 0.60 V vs. RHE. Therefore, the GOR reaction products were evaluated by HPLC and FTIR analyses. Thus, the qualitative products distribution obtained with the UV-Vis detector after 4 hours of

electrolysis at 0.55 V vs. RHE is shown in **Figure 4b**. This potential value was chosen taking into consideration the prospective effect of the Rh on fuel cell devices application. The main identified product was glycerate (29%), however, formate (13%), tartronate (8%), and oxalate (6%) are detected at low concentrations. This result is consistent with the products distribution reported in heterogeneous catalysis on the same type of material [50]. The presence of the formate ions clearly highlights the ability of Rh for the C-C bond cleavage in the glycerol molecule at low potential. Nevertheless, the presence of hydroxypyruvic acid during the electrolysis performance was not conclusive due to the retention time being very close to the tartronic acid in our chromatographic operation conditions.

The accepted GOR reaction mechanism follows two pathways involving glyceraldehyde and/or DHA (dihydroxyacetone) routes [81, 82]. Consequently, as confirmed in **Figure 4b**, the large glycerate amount indicates that the GOR on Rh/C follows the glyceraldehyde pathway. However, both species (DHA and glyceraldehyde) are unstable in high pH conditions due to the aldolization reaction [59], which difficultes their detection by HPLC [83]. Otherwise, we accomplished FTIRS measurements to identify the intermediate species resulting from glycerol oxidation on Rh/C.

In Situ Infrared Reflectance Spectroscopy Measurements

Figure 4c shows the SPAIR spectra during the 0.20 mol L^{-1} glycerol oxidation in 0.10 mol L^{-1} NaOH. The band around 1845 cm^{-1} at 0.15 V vs. RHE indicates the CO_B adsorbed formation, which confirms the glycerol dissociative adsorption at low potentials [84]. The band at 2345 cm^{-1} (starting at 0.15 V vs. RHE) corresponds to the CO_2 formation, which is related to the pH change in the thin layer, promoting a decrease in the OH^- concentration

and, consequently, glycerol is forced to react with water [85]. Later on, at 0.55 V vs. RHE a band appears at 1583 cm^{-1}, indicating the presence of different carboxylate ions in this potential region, notably glycerate [47, 84-86]. Additionally, it is important to stress that this band is also characteristic of tartronate and/or mesoxalate [87]. The band at 1386 cm^{-1} can be assigned to CO_3^{2-} formation at the beginning of the glycerol oxidation (Reference spectrum is presented in the supplementary material **(Figure 4S)).** Furthermore, carbonate formation at lower potentials was previously associated with the glycolate and oxalate production [88]. Indeed, still at 0.55 V vs. RHE, the sharp band at 1308 cm^{-1} can be assigned to oxalate confirming its formation [89]. Afterwards, at 0.65 V vs RHE, the formation of glycerate (1111 cm^{-1}) and glycolate (1074 cm^{-1}) increases [47, 84, 85]. Finally, at higher potentials (0.80 – 1.20 V vs. RHE), the shape of the broad band in the spectral range around 1300 cm^{-1} changes and the vibration bands characteristic of formate become visible namely the band at 1352 cm^{-1}.

Thereafter, we employed the SPAIRS method accumulation of spectra by coupling with a chronoamperometry experiment recorded in the spectroelectrochemical cell under the same conditions of electrolysis. **Figure 4d** depicts the FTIR spectra for glycerol oxidation at 0.55 V vs RHE during 30 min. At this potential characteristic bands to CO_B adsorbed on Rh site (1846 cm^{-1}), oxalate (1308 cm^{-1}), glycolate (1074 cm^{-1}), and glycerate (1583 cm^{-1}) were observed [47, 84-86]. Moreover, the herein observed band at 1220 cm^{-1} was attributed to adsorbed glyceraldehyde by Holade *et al*. [59].The presence of CO_B emphasizes the ability of Rh to improve the C-C bond cleavage at low potentials [50]. Based on these results, we can conclude the glyceraldehyde pathway for the glycerol electroconversion in alkaline medium on Rh/C highlighting adsorbed glycerate and glyceraldehyde as intermediates.

Additionally, the glycerol oxidation reaction scheme over Rh/C catalyst was proposed and illustrated in **Figure 5**. Firstly, during the beginning of GOR, Glycerol is initially converted into glyceraldehyde, unstable in alkaline medium, and sequentially oxidized to glycerate. Eventually, the glycerate was rapidly oxidized into tartronate and/or glycolate, indicating C-C cleavage. The formed glycolate is then converted to oxalate with carbonate formation at low potentials [88]. Nevertheless, the glycerate conversion also allows the formate production [90] as also confirmed by HPLC quantification. Furthermore, Holade *et al.* [59] described that the formate also occurs on CO adsorbed conditions as herein demonstrated CO_B presence (0.55 V vs. RHE) in **Figure 4d** at same time that HPLC formate quantification in **Figure 4b** (0.55 V vs. RHE).

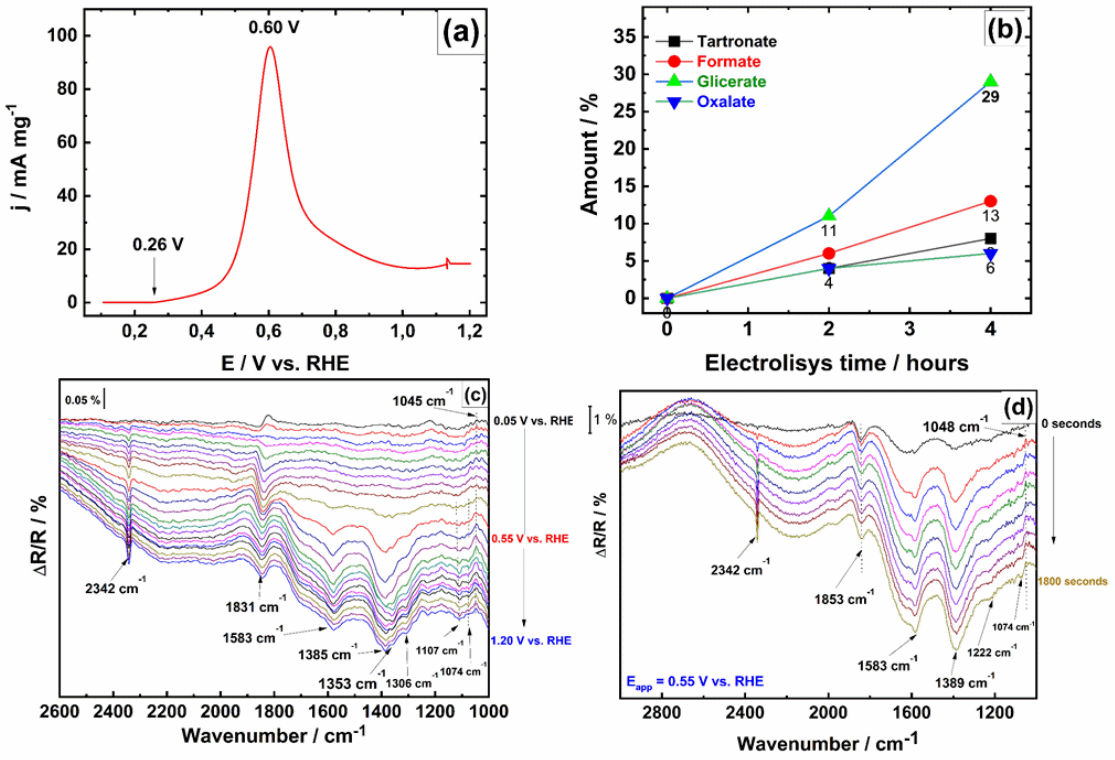

Figure 4: (a) Polarization curve of glycerol oxidation on Rh/C at 10 mV s^{-1} in 0.1 mol L^{-1} NaOH electrolytic solution containing 0.2 mol L^{-1} of glycerol; **(b)** SPAIR spectra recorded in 0.1 mol L^{-1} NaOH electrolyte containing 0.2 mol L^{-1} glycerol at 1 mV s^{-1} and in the potential range 0.10 - 1.20 V vs RHE; **(c)** FTIR spectra recorded during chronoamperometry in 0.1 mol L^{-1} NaOH + 0.2 mol L^{-1} glycerol at 0.55 V *vs.* RHE.

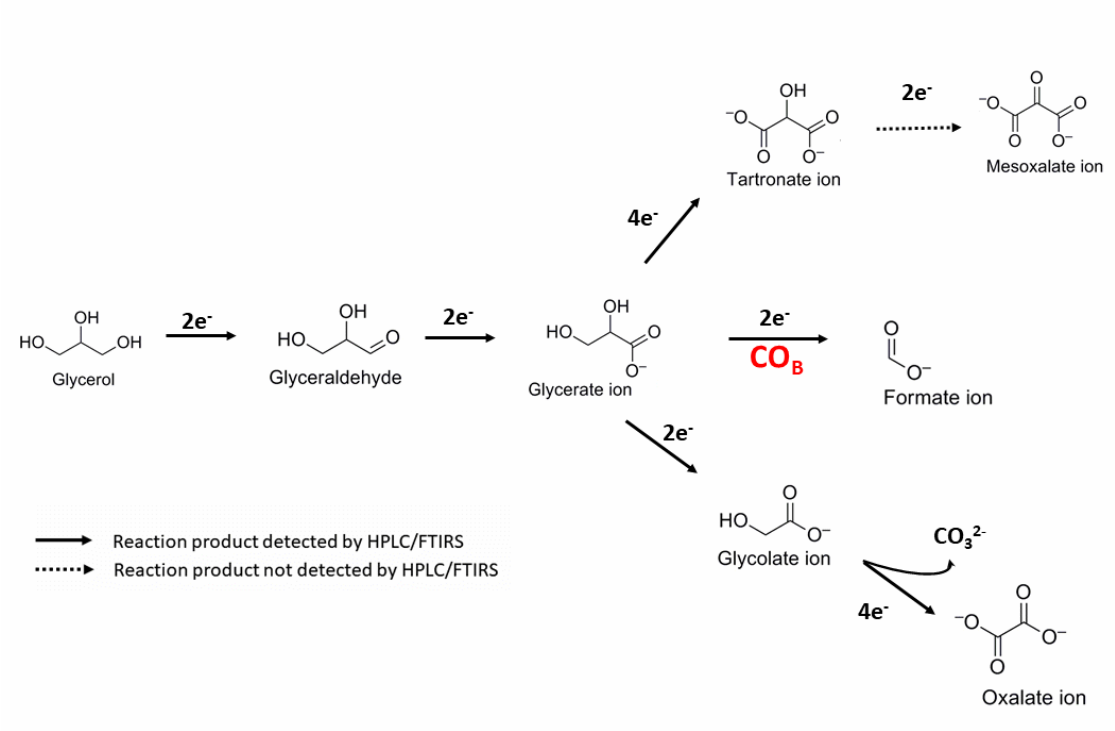

Figure 5: Reaction pathway scheme for GOR on Rh/C catalyst in alkaline medium

4 Conclusion

In the present study, Rh/C catalysts were successfully prepared following the BAE method and applied for ethanol and glycerol electro-oxidation. The physical characterizations showed that the obtained materials were composed of 2.9 nm crystallite size. XPS measurements revealed the presence of Rh^0 and Rh^{III} on the catalyst surface. The CO striping measurement coupled with *in situ* FTIR experiments revealed the presence of two well-defined bands attributed to the linearly adsorbed (CO_L) and bridged bonded CO (CO_B) on Rh sites. The potential dependence of ν(CO) frequencies for CO_L and CO_B demonstrated that the CO_L oxidation starts first at 0.35 V *vs*. RHE. The Rh effect in EOR consists of the dissociative ethanol adsorption favoring the C-C bond cleavage at low potential. The major intermediate species detected were acetate and CO_3^{2-} in both applied potential conditions (0.55 and 0.85 V vs. RHE). Therefore, on Rh/C, EOR follows two pathways in the alkaline medium. The GOR results evidenced that Rh was active towards this reaction in an alkaline medium. The reaction products obtained by two complementary techniques (HPLC and in situ FTIRS) revealed that glycerate was the main product. The results indicate that on Rh/C catalysts, the reaction follows the glyceraldehyde pathway. Overall, these insights will contribute to developing fuel cell materials for energy conversion and value-added chemicals cogeneration systems.

Acknowledgements

The authors thank CAPES-COFECUB (project n° 914/18) and CNPq for their financial support. "This study was financed in part by the Coordenação de Aperfeiçoamento de Pessoal de Nível Superior - Brasil (CAPES) - Finance Code 001". The authors also thank the European Union (ERDF) and “Région Nouvelle-Aquitaine for their financial support.

References

[1] E. Antolini, Catalysts for direct ethanol fuel cells, J. Power Sources, 170 (2007) 1-12. doi: 10.1016/j.jpowsour.2007.04.009.
[2] M.A.F. Akhairi, S.K. Kamarudin, Catalysts in direct ethanol fuel cell (DEFC): An overview, Int. J. Hydrogen Energy, 41 (2016) 4214-4228. doi: 10.1016/j.ijhydene.2015.12.145.
[3] O.Z. Sharaf, M.F. Orhan, An overview of fuel cell technology: Fundamentals and applications, Renew. Sustain. Energy Rev., 32 (2014) 810-853. doi: 10.1016/j.rser.2014.01.012.
[4] K.I. Ozoemena, S. Chen, Nanomaterials for fuel cell catalysis, Springer International Publishing, Cham, 2016.
[5] C. Li, K. Wang, D. Xie, A review of approaches for the design of high-performance electrocatalysts for ethanol electrooxidation, Surfaces and Interfaces, (2021) 101594. doi: https://doi.org/10.1016/j.surfin.2021.101594.
[6] S.P.S. Badwal, S. Giddey, A. Kulkarni, J. Goel, S. Basu, Direct ethanol fuel cells for transport and stationary applications – A comprehensive review, Applied Energy, 145 (2015) 80-103. doi: 10.1016/j.apenergy.2015.02.002.
[7] S. Samad, K.S. Loh, W.Y. Wong, T.K. Lee, J. Sunarso, S.T. Chong, W.R. Wan Daud, Carbon and non-carbon support materials for platinum-based catalysts in fuel cells, Int. J. Hydrogen Energy, 43 (2018) 7823-7854. doi: 10.1016/J.IJHYDENE.2018.02.154.
[8] E. Ferreira Frota, V.V. Silva de Barros, B.R.S. de Araújo, Â. Gonzaga Purgatto, J.J. Linares, Pt/C containing different platinum loadings for use as electrocatalysts in alkaline PBI-based direct glycerol fuel cells, International Journal of Hydrogen Energy, 42 (2017) 23095-23106. doi: 10.1016/J.IJHYDENE.2017.07.125.

[9] S. Guo, E. Wang, Noble metal nanomaterials: Controllable synthesis and application in fuel cells and analytical sensors, Nano Today, 6 (2011) 240-264. doi: http://dx.doi.org/10.1016/j.nantod.2011.04.007.
[10] S.Q. Song, W.J. Zhou, Z.H. Zhou, L.H. Jiang, G.Q. Sun, Q. Xin, V. Leontidis, S. Kontou, P. Tsiakaras, Direct ethanol PEM fuel cells: The case of platinum based anodes, Int. J. Hydrogen Energy, 30 (2005) 995-1001. doi: 10.1016/j.ijhydene.2004.11.006.
[11] S. Sen Gupta, S.S. Mahapatra, J. Datta, A potential anode material for the direct alcohol fuel cell, J. Power Sources, 131 (2004) 169-174. doi.
[12] R.M. Antoniassi, L. Otubo, J.M. Vaz, A. Oliveira Neto, E.V. Spinacé, Synthesis of Pt nanoparticles with preferential (100) orientation directly on the carbon support for Direct Ethanol Fuel Cell, J. Catal., 342 (2016) 67-74. doi: 10.1016/j.jcat.2016.07.022.
[13] A. Mondal, A. De, J. Datta, Selective methodology for developing PtCo NPs and performance screening for energy efficient electro-catalysis in direct ethanol fuel cell, International Journal of Hydrogen Energy, 44 (2019) 10996-11011. doi: 10.1016/J.IJHYDENE.2019.02.146.
[14] W. Wang, X. Liu, Y. Wang, L. Zhang, S. Imhanria, Z. Lei, A metal–organic framework derived PtCo/C electrocatalyst for ethanol electro-oxidation, Journal of the Taiwan Institute of Chemical Engineers, 104 (2019) 284-292. doi: 10.1016/J.JTICE.2019.08.015.
[15] H. Yan, S. Yao, B. Yin, W. Liang, X. Jin, X. Feng, Y. Liu, X. Chen, C. Yang, Synergistic effects of bimetallic PtRu/MCM-41 nanocatalysts for glycerol oxidation in base-free medium: Structure and electronic coupling dependent activity, Applied Catalysis B: Environmental, 259 (2019) 118070-118070. doi: 10.1016/J.APCATB.2019.118070.
[16] R.M. Altarawneh, P.G. Pickup, Pt and PtRu catalyst bilayers increase efficiencies for ethanol oxidation in proton exchange membrane electrolysis and fuel cells, Journal of Power Sources, 366 (2017) 27-32. doi: 10.1016/J.JPOWSOUR.2017.09.014.
[17] I.H. Ko, W.D. Lee, J.Y. Baek, Y.E. Sung, H.I. Lee, Modified polyol method for a highly alloyed PtRu/C electrocatalyst: Effect of hot injection of metal precursor and NaOH, Materials Chemistry and Physics, 183 (2016) 11-17. doi: 10.1016/j.matchemphys.2016.05.052.
[18] G. Chen, X. Yang, Z. Xie, F. Zhao, Z. Zhou, Q. Yuan, Hollow PtCu octahedral nanoalloys: Efficient bifunctional electrocatalysts towards oxygen reduction reaction and methanol oxidation reaction by regulating near-surface composition, Journal of Colloid and Interface Science, 562 (2020) 244-251. doi: 10.1016/J.JCIS.2019.12.020.
[19] C. Liu, L. Zhang, L. Sun, W. Wang, Z. Chen, Enhanced electrocatalytic activity of PtCu bimetallic nanoparticles on CeO2/carbon nanotubes for methanol electro-oxidation, International Journal of Hydrogen Energy, 45 (2020) 8558-8567. doi: 10.1016/J.IJHYDENE.2020.01.063.
[20] R.M. Castagna, J.M. Sieben, A.E. Alvarez, M.M.E. Duarte, Electrooxidation of ethanol and glycerol on carbon supported PtCu nanoparticles, International

Journal of Hydrogen Energy, 44 (2019) 5970-5982. doi: 10.1016/J.IJHYDENE.2019.01.090.
[21] J. Maya-Cornejo, R. Carrera-Cerritos, D. Sebastián, J. Ledesma-García, L.G. Arriaga, A.S. Aricò, V. Baglio, PtCu catalyst for the electro-oxidation of ethanol in an alkaline direct alcohol fuel cell, International Journal of Hydrogen Energy, 42 (2017) 27919-27928. doi: 10.1016/J.IJHYDENE.2017.07.226.
[22] H. Song, M. Luo, X. Qiu, G. Cao, Insights into the endurance promotion of PtSn/CNT catalysts by thermal annealing for ethanol electro-oxidation, Electrochimica Acta, 213 (2016) 578-586. doi: 10.1016/J.ELECTACTA.2016.07.053.
[23] E. Antolini, E.R. Gonzalez, Effect of synthesis method and structural characteristics of Pt–Sn fuel cell catalysts on the electro-oxidation of CH3OH and CH3CH2OH in acid medium☆, Catal. Today, 160 (2011) 28-38. doi: 10.1016/j.cattod.2010.07.018.
[24] B. Fang, Z. Liu, Y. Bao, L. Feng, Unstable Ni leaching in MOF-derived PtNi-C catalyst with improved performance for alcohols fuel electro-oxidation, Chinese Chemical Letters, (2020). doi: 10.1016/J.CCLET.2020.02.045.
[25] Y. Holade, R.G. da Silva, K. Servat, T.W. Napporn, C. Canaff, A.R. de Andrade, K.B. Kokoh, Facile synthesis of highly active and durable PdM/C (M = Fe, Mn) nanocatalysts for the oxygen reduction reaction in an alkaline medium, J. Mater. Chem. A, 4 (2016) 8337-8349. doi: 10.1039/C6TA02096H.
[26] M.C. Moraes, G.G. Junco, T.F.M. Moreira, C.J.G. Pinheiro, P. Olivi, D. Profeti, L.P.R. Profeti, NiO-promoted Pt electrocatalysts prepared by thermal decomposition of polymeric precursors for oxidation of glycerol in alkaline medium, Journal of Environmental Chemical Engineering, 7 (2019) 102922-102922. doi: 10.1016/j.jece.2019.102922.
[27] R.G. Da Silva, S. Aquino Neto, K.B. Kokoh, A.R. De Andrade, Electroconversion of glycerol in alkaline medium: From generation of energy to formation of value-added products, J. Power Sources, 351 (2017) 174-182. doi: http://doi.org/10.1016/j.jpowsour.2017.03.101.
[28] T. Jiang, Q. Huai, T. Geng, W. Ying, T. Xiao, F. Cao, Catalytic performance of Pd–Ni bimetallic catalyst for glycerol hydrogenolysis, Biomass Bioenerg., 78 (2015) 71-79. doi: 10.1016/J.BIOMBIOE.2015.04.017.
[29] R.M. Altarawneh, T.M. Brueckner, B. Chen, P.G. Pickup, Product distributions and efficiencies for ethanol oxidation at PtNi octahedra, J. Power Sources, 400 (2018) 369-376. doi: 10.1016/J.JPOWSOUR.2018.08.052.
[30] S.T. Nguyen, Y. Yang, X. Wang, Ethanol electro-oxidation activity of Nb-doped-TiO2 supported PdAg catalysts in alkaline media, Applied Catalysis B: Environmental, 113-114 (2012) 261-270. doi: 10.1016/J.APCATB.2011.11.046.
[31] W.J. Pech-Rodríguez, D. González-Quijano, G. Vargas-Gutiérrez, C. Morais, T.W. Napporn, F.J. Rodríguez-Varela, Electrochemical and in situ FTIR study of the ethanol oxidation reaction on PtMo/C nanomaterials in alkaline media, Applied Catalysis B: Environmental, 203 (2017) 654-662. doi: 10.1016/J.APCATB.2016.10.058.
[32] E.S. Valério Neto, M.A. Gomes, G.R. Salazar-Banda, K.I.B. Eguiluz, Pt and Pt–Rh nanowires supported on carbon and SnO2:Sb nanoparticles for ethanol

electrochemical oxidation in acidic media, International Journal of Hydrogen Energy, 43 (2018) 178-188. doi: 10.1016/J.IJHYDENE.2017.11.014.
[33] J. Lu, L. Zhang, S. Jing, L. Luo, S. Yin, Remarkably efficient PtRh alloyed with nanoscale WC for hydrogen evolution in alkaline solution, Int. J. Hydrogen Energy, 42 (2017) 5993-5999. doi: 10.1016/j.ijhydene.2017.01.181.
[34] L.A. Soares, C. Morais, T.W. Napporn, K.B. Kokoh, P. Olivi, Beneficial effects of rhodium and tin oxide on carbon supported platinum catalysts for ethanol electrooxidation, J. Power Sources, 315 (2016) 47-55. doi: http://dx.doi.org/10.1016/j.jpowsour.2016.03.013.
[35] P. Mukherjee, P.S. Roy, S.K. Bhattacharya, Improved carbonate formation from ethanol oxidation on nickel supported Pt–Rh electrode in alkaline medium at room temperature, Int. J. Hydrogen Energy, 40 (2015) 13357-13367. doi: 10.1016/j.ijhydene.2015.07.154.
[36] Y.-W. Lee, K.-W. Park, Pt–Rh alloy nanodendrites for improved electrocatalytic activity and stability in methanol electrooxidation reaction, Catalysis Communications, 55 (2014) 24-28. doi: https://doi.org/10.1016/j.catcom.2014.06.009.
[37] M. Li, W.P. Zhou, N.S. Marinkovic, K. Sasaki, R.R. Adzic, The role of rhodium and tin oxide in the platinum-based electrocatalysts for ethanol oxidation to CO2, Electrochimica Acta, 104 (2013) 454-461. doi: 10.1016/j.electacta.2012.10.046.
[38] C. Zhu, S. Guo, S. Dong, PdM (M = Pt, Au) Bimetallic Alloy Nanowires with Enhanced Electrocatalytic Activity for Electro-oxidation of Small Molecules, Advanced Materials, 24 (2012) 2326-2331. doi: 10.1002/adma.201104951.
[39] R.F.B. De Souza, A.E.A. Flausino, D.C. Rascio, R.T.S. Oliveira, E.T. Neto, M.L. Calegaro, M.C. Santos, Ethanol oxidation reaction on PtCeO2/C electrocatalysts prepared by the polymeric precursor method, Applied Catalysis B: Environmental, 91 (2009) 516-523. doi: 10.1016/J.APCATB.2009.06.022.
[40] G. Tremiliosi-Filho, E.R. Gonzalez, A.J. Motheo, E.M. Belgsir, J.M. Léger, C. Lamy, Electro-oxidation of ethanol on gold: analysis of the reaction products and mechanism, J. Electroanal. Chem., 444 (1998) 31-39. doi.
[41] F. Alcaide, G. Álvarez, P.L. Cabot, R.V. Genova-Koleva, H.-J. Grande, M.V. Martínez-Huerta, O. Miguel, Supporting PtRh alloy nanoparticle catalysts by electrodeposition on carbon paper for the ethanol electrooxidation in acidic medium, Journal of Electroanalytical Chemistry, 861 (2020) 113960-113960. doi: 10.1016/J.JELECHEM.2020.113960.
[42] J. Bai, X. Xiao, Y.-Y. Xue, J.-X. Jiang, J.-H. Zeng, X.-F. Li, Y. Chen, Bimetallic Platinum–Rhodium Alloy Nanodendrites as Highly Active Electrocatalyst for the Ethanol Oxidation Reaction, ACS Applied Materials & Interfaces, 10 (2018) 19755-19763. doi: 10.1021/acsami.8b05422.
[43] F. Zhu, K. Tu, L. Huang, X. Qu, J. Zhang, H. Liao, Z. Zhou, Y. Jiang, S. Sun, High selectivity PtRh/RGO catalysts for ethanol electro-oxidation at low potentials: Enhancing the efficiency of CO2 from alcoholic groups, Electrochimica Acta, 292 (2018) 208-216. doi: https://doi.org/10.1016/j.electacta.2018.08.142.

[44] P. Wang, Y. Wen, S. Yin, N. Wang, PtRh alloys on hybrid TiO 2 e Carbon support as high efficiency catalyst for ethanol oxidation, Int. J. Hydrogen Energy, 42 (2017) 24689-24696. doi: 10.1016/j.ijhydene.2017.04.302.
[45] L. Rao, Y.-X. Jiang, B.-W. Zhang, Y.-R. Cai, S.-G. Sun, High activity of cubic PtRh alloys supported on graphene towards ethanol electrooxidation, Physical Chemistry Chemical Physics, 16 (2014) 13662-13662. doi: 10.1039/c3cp55059a.
[46] S. Sen Gupta, J. Datta, A comparative study on ethanol oxidation behavior at Pt and PtRh electrodeposits, J. Electroanal. Chem., 594 (2006) 65-72. doi.
[47] L. Huang, J.-Y. Sun, S.-H. Cao, M. Zhan, Z.-R. Ni, H.-J. Sun, Z. Chen, Z.-Y. Zhou, E.G. Sorte, Y.J. Tong, S.-G. Sun, Combined EC-NMR and In Situ FTIR Spectroscopic Studies of Glycerol Electrooxidation on Pt/C, PtRu/C, and PtRh/C, ACS Catalysis, 6 (2016) 7686-7695. doi: 10.1021/acscatal.6b02097.
[48] F. Zhang, D. Zhou, Z. Zhang, M. Zhou, Q. Wang, Preparation of Rh/C and its high electro-catalytic activity for ethanol oxidation in alkaline media, RSC Advances, 5 (2015) 91829-91835. doi: 10.1039/C5RA16859G.
[49] Y. Suo, I.M. Hsing, Highly active rhodium/carbon nanocatalysts for ethanol oxidation in alkaline medium, Journal of Power Sources, 196 (2011) 7945-7950. doi: https://doi.org/10.1016/j.jpowsour.2011.05.048.
[50] E.G. Rodrigues, S.A.C. Carabineiro, X. Chen, J.J. Delgado, J.L. Figueiredo, M.F.R. Pereira, J.J.M. Órfão, Selective Oxidation of Glycerol Catalyzed by Rh/Activated Carbon: Importance of Support Surface Chemistry, Catal. Lett., 141 (2011) 420-431. doi: 10.1007/s10562-010-0515-9.
[51] J.P.I. De Souza, S.L. Queiroz, K. Bergamaski, E.R. Gonzalez, F.C. Nart, Electro-oxidation of ethanol on Pt, Rh, and PtRh electrodes. A study using DEMS and in-situ FTIR techniques, Journal of Physical Chemistry B, 106 (2002) 9825-9830. doi: 10.1021/jp014645c.
[52] E.H. Fontes, R.M. Piasentin, J.M.S. Ayoub, J.C.M. da Silva, M.H.M.T. Assumpção, E.V. Spinacé, A.O. Neto, R.F.B. de Souza, Electrochemical and in situ ATR-FTIR studies of ethanol electro-oxidation in alkaline medium using PtRh/C electrocatalysts, Materials for Renewable and Sustainable Energy, 4 (2015) 3-3. doi: 10.1007/s40243-015-0043-z.
[53] J.-Y. Ye, Y.-X. Jiang, T. Sheng, S.-G. Sun, In-situ FTIR spectroscopic studies of electrocatalytic reactions and processes, Nano Energy, 29 (2016) 414-427. doi: https://doi.org/10.1016/j.nanoen.2016.06.023.
[54] D.R.M. Godoi, H.M. Villullas, F.-C. Zhu, Y.-X. Jiang, S.-G. Sun, J. Guo, L. Sun, R. Chen, A comparative investigation of metal-support interactions on the catalytic activity of Pt nanoparticles for ethanol oxidation in alkaline medium, J. Power Sources, 311 (2016) 81-90. doi: 10.1016/j.jpowsour.2016.02.011.
[55] K.L. Bhowmik, A. Debnath, R.K. Nath, S. Das, K.K. Chattopadhyay, B. Saha, Synthesis and characterization of mixed phase manganese ferrite and hausmannite magnetic nanoparticle as potential adsorbent for methyl orange from aqueous media: Artificial neural network modeling, Journal of Molecular Liquids, 219 (2016) 1010-1022. doi: 10.1016/j.molliq.2016.04.009.
[56] S. Beyhan, J.-M. Léger, F. Kadırgan, Understanding the influence of Ni, Co, Rh and Pd addition to PtSn/C catalyst for the oxidation of ethanol by in situ

Fourier transform infrared spectroscopy, Applied Catalysis B: Environmental, 144 (2014) 66-74. doi: 10.1016/J.APCATB.2013.07.020.
[57] P.S. Fernández, C.A. Martins, M.E. Martins, G.A. Camara, Electrooxidation of glycerol on platinum nanoparticles: Deciphering how the position of each carbon affects the oxidation pathways, Electrochimica Acta, 112 (2013) 686-691. doi: 10.1016/J.ELECTACTA.2013.09.032.
[58] Y. Holade, K. Servat, T.W. Napporn, K.B. Kokoh, Electrocatalytic properties of nanomaterials synthesized from "Bromide Anion Exchange" method - Investigations of glucose and glycerol oxidation, Electrochimica Acta, 162 (2015) 205-214. doi: 10.1016/j.electacta.2014.11.072.
[59] Y. Holade, C. Morais, K. Servat, T.W. Napporn, K.B. Kokoh, Toward the Electrochemical Valorization of Glycerol: Fourier Transform Infrared Spectroscopic and Chromatographic Studies, ACS Catalysis, 3 (2013) 2403-2411. doi: 10.1021/cs400559d.
[60] T.F. Messa Moreira, S.A. Neto, C. Lemoine, K.B. Kokoh, C. Morais, T.W. Napporn, P. Olivi, Rhodium effects on Pt anode materials in a direct alkaline ethanol fuel cell, RSC Advances, 10 (2020) 35310-35317. doi: 10.1039/D0RA06570F.
[61] E.N. El Sawy, P.G. Pickup, Carbon monoxide and formic acid oxidation at Rh@Pt nanoparticles, Electrochimica Acta, 302 (2019) 234-240. doi: https://doi.org/10.1016/j.electacta.2019.02.047.
[62] L. Rao, Y.-X. Jiang, B.-W. Zhang, Y.-R. Cai, S.-G. Sun, High activity of cubic PtRh alloys supported on graphene towards ethanol electrooxidation, Phys. Chem. Chem. Phys., 16 (2014) 13662-13671. doi: 10.1039/C3CP55059A.
[63] G. Jerkiewicz, J.J. Borodzinski, Relation between the surface states of oxide films at Rh electrodes and kinetics of the oxygen evolution reaction, Journal of the Chemical Society, Faraday Transactions, 90 (1994) 3669-3675. doi: 10.1039/FT9949003669.
[64] G. Jerkiewicz, J.J. Borodzinski, Studies of formation of very thin oxide films on polycrystalline rhodium electrodes: application of the Mott-Cabrera theory, Langmuir, 9 (1993) 2202-2209. doi: 10.1021/la00032a049.
[65] I. Yruela, S.I. Allakhverdiev, J.V. Ibarra, V.V. Klimov, Bicarbonate binding to the water-oxidizing complex in the photosystem II. A Fourier transform infrared spectroscopy study 1, FEBS Letters, 425 (1998) 396-400. doi: 10.1016/S0014-5793(98)00271-3.
[66] H. Yoshida, S. Narisawa, S.-i. Fujita, L. Ruixia, M. Arai, In situ FTIR study on the formation and adsorption of CO on alumina-supported noble metal catalysts from H2 and CO2 in the presence of water vapor at high pressures, Physical Chemistry Chemical Physics, 14 (2012) 4724-4733. doi: 10.1039/C2CP23590K.
[67] K.I. Hadjivanov, G.N. Vayssilov, Characterization of Oxide Surfaces and Zeolites by Carbon Monoxide as an IR Probe Molecule, ChemInform, 34 (2003). doi: 10.1002/chin.200317296.
[68] J. Raskó, J. Bontovics, FTIR study of the rearrangement of adsorbed CO species on Al2O3-supported rhodium catalysts, Catalysis Letters, 58 (1999) 27-32. doi: 10.1023/A:1019053228217.

[69] M. Frank, R. Kühnemuth, M. Bäumer, H.-J. Freund, Vibrational spectroscopy of CO adsorbed on supported ultra-small transition metal particles and single metal atoms, Surface Science, 454-456 (2000) 968-973. doi: https://doi.org/10.1016/S0039-6028(00)00241-7.
[70] C.R.K. Rao, D.C. Trivedi, Chemical and electrochemical depositions of platinum group metals and their applications, Coordination Chemistry Reviews, 249 (2005) 613-631. doi: https://doi.org/10.1016/j.ccr.2004.08.015.
[71] Y. Kang, F. Li, S. Li, P. Ji, J. Zeng, J. Jiang, Y. Chen, Unexpected catalytic activity of rhodium nanodendrites with nanosheet subunits for methanol electrooxidation in an alkaline medium, Nano Research, 9 (2016) 3893-3902. doi: 10.1007/s12274-016-1258-8.
[72] A. Bach Delpeuch, F. Maillard, M. Chatenet, P. Soudant, C. Cremers, Ethanol oxidation reaction (EOR) investigation on Pt/C, Rh/C, and Pt-based bi- and tri-metallic electrocatalysts: A DEMS and in situ FTIR study, Applied Catalysis B: Environmental, 181 (2016) 672-680. doi: https://doi.org/10.1016/j.apcatb.2015.08.041.
[73] G.L. Caneppele, C.A. Martins, Revisiting glycerol electrooxidation by applying derivative voltammetry: From well-ordered bulk Pt to bimetallic nanoparticles, Journal of Electroanalytical Chemistry, (2020) 114139-114139. doi: 10.1016/J.JELECHEM.2020.114139.
[74] E.H. Fontes, C.E.D. Ramos, J. Nandenha, R.M. Piasentin, A.O. Neto, R. Landers, Structural analysis of PdRh/C and PdSn/C and its use as electrocatalysts for ethanol oxidation in alkaline medium, International Journal of Hydrogen Energy, 44 (2019) 937-951. doi: 10.1016/J.IJHYDENE.2018.11.049.
[75] T. Sheng, W.-F. Lin, C. Hardacre, P. Hu, Significance of β-dehydrogenation in ethanol electro-oxidation on platinum doped with Ru, Rh, Pd, Os and Ir, Physical Chemistry Chemical Physics, 16 (2014) 13248-13254. doi: 10.1039/C4CP00737A.
[76] K. Bergamaski, E.R. Gonzalez, F.C. Nart, Ethanol oxidation on carbon supported platinum-rhodium bimetallic catalysts, Electrochimica Acta, 53 (2008) 4396-4406. doi.
[77] H. Siwek, W. Tokarz, P. Piela, A. Czerwiński, Electrochemical behavior of CO, CO2 and methanol adsorption products formed on Pt–Rh alloys of various surface compositions, J. Power Sources, 181 (2008) 24-30. doi: https://doi.org/10.1016/j.jpowsour.2007.11.033.
[78] D.A. Cantane, W.F. Ambrosio, M. Chatenet, F.H.B. Lima, Electro-oxidation of ethanol on Pt/C, Rh/C, and Pt/Rh/C-based electrocatalysts investigated by on-line DEMS, Journal of Electroanalytical Chemistry, 681 (2012) 56-65. doi: https://doi.org/10.1016/j.jelechem.2012.05.024.
[79] S. Beyhan, J.-M. Léger, F. Kadırgan, Adsorption and oxidation of acetaldehyde on carbon supported Pt, PtSn and PtSn-based trimetallic catalysts by in situ Fourier transform infrared spectroscopy, Journal of Power Sources, 242 (2013) 503-509. doi: https://doi.org/10.1016/j.jpowsour.2013.05.112.
[80] E. Méndez, J.L. Rodríguez, M.C. Arévalo, E. Pastor, Comparative Study of Ethanol and Acetaldehyde Reactivities on Rhodium Electrodes in Acidic Media, Langmuir, 18 (2002) 763-772. doi: 10.1021/la010747i.

[81] Y. Kang, W. Wang, Y. Pu, J. Li, D. Chai, Z. Lei, An effective Pd-NiOx-P composite catalyst for glycerol electrooxidation: Co-existed phosphorus and nickel oxide to enhance performance of Pd, Chemical Engineering Journal, 308 (2017) 419-427. doi: 10.1016/J.CEJ.2016.09.087.
[82] E. Antolini, Glycerol Electro-Oxidation in Alkaline Media and Alkaline Direct Glycerol Fuel Cells, Catalysts, 9 (2019). doi: 10.3390/catal9120980.
[83] M. Pagliaro, R. Ciriminna, H. Kimura, M. Rossi, C. Della Pina, From Glycerol to Value-Added Products, Angew. Chem. Int. Ed., 46 (2007) 4434-4440. doi: 10.1002/anie.200604694.
[84] R.S. Ferreira Jr, M. Janete Giz, G.A. Camara, Influence of the local pH on the electrooxidation of glycerol on Palladium–Rhodium electrodeposits, Journal of Electroanalytical Chemistry, 697 (2013) 15-20. doi: https://doi.org/10.1016/j.jelechem.2013.03.007.
[85] D.Z. Jeffery, G.A. Camara, The formation of carbon dioxide during glycerol electrooxidation in alkaline media: First spectroscopic evidences, Electrochemistry Communications, 12 (2010) 1129-1132. doi: https://doi.org/10.1016/j.elecom.2010.06.001.
[86] M. Simões, S. Baranton, C. Coutanceau, Enhancement of catalytic properties for glycerol electrooxidation on Pt and Pd nanoparticles induced by Bi surface modification, Applied Catalysis B: Environmental, 110 (2011) 40-49. doi: https://doi.org/10.1016/j.apcatb.2011.08.020.
[87] V.L. Oliveira, C. Morais, K. Servat, T.W. Napporn, G. Tremiliosi-Filho, K.B. Kokoh, Glycerol oxidation on nickel based nanocatalysts in alkaline medium – Identification of the reaction products, Journal of Electroanalytical Chemistry, 703 (2013) 56-62. doi: https://doi.org/10.1016/j.jelechem.2013.05.021.
[88] T. Hu, Y. Wang, Q. Liu, L. Zhang, H. Wang, T. Tang, W. Chen, M. Zhao, J. Jia, In-situ synthesis of palladium-base binary metal oxide nanoparticles with enhanced electrocatalytic activity for ethylene glycol and glycerol oxidation, Int. J. Hydrogen Energy, 42 (2017) 25951-25959. doi: https://doi.org/10.1016/j.ijhydene.2017.08.160.
[89] L. Demarconnay, S. Brimaud, C. Coutanceau, J.M. Léger, Ethylene glycol electrooxidation in alkaline medium at multi-metallic Pt based catalysts, Journal of Electroanalytical Chemistry, 601 (2007) 169-180. doi: https://doi.org/10.1016/j.jelechem.2006.11.006.
[90] C. Liu, M. Hirohara, T. Maekawa, R. Chang, T. Hayashi, C.-Y. Chiang, Selective electro-oxidation of glycerol to dihydroxyacetone by a non-precious electrocatalyst – CuO, Applied Catalysis B: Environmental, 265 (2020) 118543. doi: https://doi.org/10.1016/j.apcatb.2019.118543.